Mechanistic Origins of the Substrate Selectivity of Serine Proteases

April Case and Ross L. Stein*

Laboratory for Drug Discovery in Neurodegeneration, Harvard Center for Neurodegeneration and Repair, 65 Landsdowne Street, Fourth Floor, Cambridge, Massachusetts 02139

Received November 19, 2002; Revised Manuscript Received January 2, 2003

ABSTRACT: Serine proteases catalyze the hydrolysis of amide bonds of their protein and peptide substrates through a mechanism involving the intermediacy of an acyl−enzyme. While the rate constant for formation of this intermediate, k_2, shows a dramatic dependence on peptide chain length, the rate constant for the intermediate's hydrolysis is relatively insensitive to chain length. To probe the mechanistic origins of this phenomenon, we determined temperature dependencies and solvent isotope effects for the α-chymotrypsin-catalyzed hydrolysis of Suc-Phe-pNA ($K_s = 1$ mM, $k_2 = 0.04$ s^{-1}, and $k_3 = 11$ s^{-1}), Suc-Ala-Phe-pNA ($K_s = 4$ mM, $k_2 = 0.9$ s^{-1}, and $k_3 = 42$ s^{-1}), and Suc-Ala-Ala-Pro-Phe-pNA ($K_s = 0.1$ mM, $k_2 = 98$ s^{-1}, and $k_3 = 71$ s^{-1}). We found that while the van't Hoff plots for K_s and the Eyring plots for k_3 are linear for all three reactions, the Eyring plots for k_2 are convex, indicating that the process governed by k_2 is complex, possibly involving a coupling between active site chemistry and protein conformational isomerization. This interpretation is strengthened by solvent isotope effects on k_2 that are largely temperature-independent. Furthermore, the dependence of k_2 on peptide length is manifested entirely in the enthalpy of activation, suggesting a mechanism of catalysis by distortion. Taken together, this analysis of acylation suggests that extended substrates which can engage in subsite interactions are able to efficiently trigger the coupling mechanism between chemistry and a conformational isomerization that distorts the substrate and thereby promotes nucleophilic attack.

To play their role in cellular physiology, enzymes have had to develop two types of selectivity: selectivity toward the substrates they bind and selectivity toward the reactions they catalyze. While both types of selectivity are similar in that they depend on the precise orientation of active site residues, they differ in the position, along the reaction pathway, where they become expressed. Chemical selectivity is expressed entirely in catalytic transition states, whereas selectivity toward substrates can be expressed in binding, catalytic transition states, or both.

In this study, we have undertaken an investigation of the mechanistic origins of substrate selectivity.[1] In undertaking this study, we were particularly interested in first discovering which steps along the reaction pathway manifest substrate selectivity and then, if selectivity is expressed in catalytic rather than binding steps, accounting for the rate constant differences among the substrates. That is, in the case of kinetic selectivity, we will want to know if rate constant differences among the substrates are due to substrate structure-dependent changes in the rate-limiting step or differential transition-state stabilization. And, for either of these latter situations, we will want to probe their underlying kinetic and thermodynamic basis. The object we have chosen for this study is α-chymotrypsin, a well-studied member of the family of serine proteases.

Serine proteases catalyze the hydrolysis of amide bonds of their protein and peptide substrates according to the three-step mechanism of Scheme 1. In the first step, the substrate and enzyme combine to form the Michaelis complex. From within this complex, the hydroxyl of the active site serine attacks the carbonyl carbon of the amide bond of the substrate to generate an acyl−enzyme intermediate and liberate the first product. Finally, hydrolysis of the acyl−enzyme intermediate produces the reaction's second product and regenerates free enzyme. For this mechanism, the steady-state rate parameters, k_c/K_m, k_c, and K_m, are related to the mechanistic rate parameters, K_s, k_2, and k_3, as shown in eqs 1−3.

$$\frac{k_c}{K_m} = \frac{k_2}{K_s} \tag{1}$$

$$k_c = \frac{k_2 k_3}{k_2 + k_3} \tag{2}$$

$$K_m = K_s \frac{k_3}{k_2 + k_3} \tag{3}$$

In these expressions, $K_s = (k_{-1} + k_2)/k_1$, which for hydrolyses of most amides can be simplified to $K_s = k_{-1}/k_1$.

An intriguing mechanistic feature that is apparently shared by all serine proteases is the dependence of catalytic efficiency on peptide chain length. For example, it was noted by Thompson and Blout (*1*) that increasing the length of the

* To whom correspondence should be addressed: Laboratory for Drug Discovery in Neurodegeneration, Harvard Center for Neurodegeneration and Repair, 65 Landsdowne St., Fourth Floor, Cambridge, MA 02139. Phone: (617) 768-8651. Fax: (617) 768-8606. E-mail: rstein@rics.bwh.harvard.edu.

[1] Confusion exists concerning the use of "selectivity" and "specificity" when discussing how an enzyme and substrate recognize and bind one another. Selectivity is a property that is possessed by the enzyme; this property empowers the enzyme to select substrates for binding and reaction. Specificity is a property that is possessed by a substrate; this property renders the substrate especially reactive toward enzyme, as manifested in kinetic parameters, especially k_c/K_m, the "specificity constant". Thus, an enzyme's substrate selectivity is, by definition, manifested toward specific substrates.

10.1021/bi020668l CCC: $25.00
Published on Web 02/28/2003

Scheme 1: Minimal Kinetic Mechanism for Serine Protease Catalysis

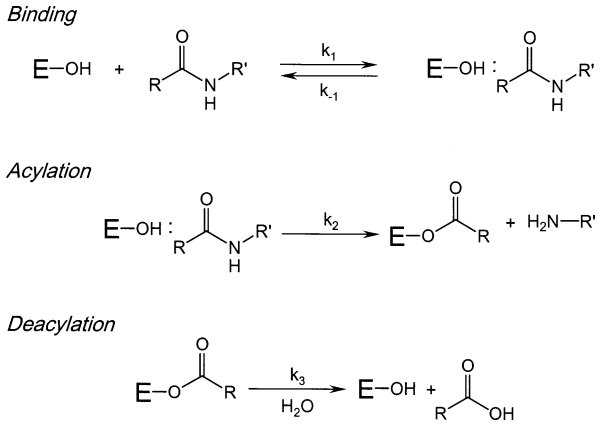

trimer Ac-Ala-Pro-Ala-NH_2 by one amino acid to produce Ac-Pro-Ala-Pro-Ala-NH_2 results in a 100-fold increase in k_c/K_m for reactions of porcine pancreatic elastase. Furthermore, this is entirely an effect on k_c, which increases from 0.1 to 9 s^{-1}, with no effect on K_m, which equals 4 mM for both substrates. Similar results were observed for the hydrolyses of a series of peptide *p*-nitroanilides by leukocyte elastase (*2*). For this system, k_c/K_m increases from 75 to 56 000 M^{-1} s^{-1} as the substrate is lengthened from Suc-Val-pNA[2] to Suc-Ala-Pro-Val-pNA. Kinetic dissection revealed that that this rate enhancement is manifested entirely in acylation: k_2 increases 1000-fold, from 0.06 to 43 s^{-1}, while K_s and k_3 remain unchanged and equal to 0.8 mM and 13 s^{-1}, respectively.

To probe the mechanistic origins of this particular aspect of chymotrypsin's selectivity toward its substrates, we determined the temperature dependencies of K_s, k_2, and k_3 for the α-CT-catalyzed hydrolyses of Suc-Phe-pNA, Suc-Ala-Phe-pNA, and Suc-Ala−Ala-Pro-Phe-pNA. For this series of reactions, selectivity is expressed nearly exclusively in k_2, and thermodynamic parameters which were determined for this parameter suggest that selectivity results entirely from a decrease in the enthalpy of activation as the substrate is lengthened. A number of mechanisms are considered to explain this.

MATERIALS AND METHODS

General

Buffer salts and deuterium oxide were from Sigma Chemical Co. Suc-Phe-pNA, Suc-Ala-Ala-Pro-Phe-pNA, and Suc-Ala-Ala-Pro-Phe-SBzl were from Bachem. Suc-Phe-SBzl, Suc-Ala-Phe-pNA, and Suc-Ala-Phe-SBzl were purchased from Absolute Science (Cambridge, MA). Substrate stock solutions were prepared in DMSO and stored at −20 °C. Bovine α-CT was a crystalline product from Sigma (C 7762) and was used without further purification. Stock solutions of α-CT were prepared in 1 mM HCl at 1 mg/mL ($[\alpha\text{-CT}]_{stock}$ = 40 μM) and stored in 1.0 mL aliquots at −20 °C. Each day's kinetic experiments were conducted with a freshly thawed aliquot of stock enzyme.

Choice of Buffer Salts for pH Dependencies

In all kinetic studies, reaction solutions contained 50 mM buffer salt, 500 mM NaCl, 10 mM $CaCl_2$, and 4% DMSO. The following buffer salts were used: acetate (pK_a = 4.8) for pH 4.5−5.5, PIPES (pK_a = 6.8) for pH 5.5−7.5, HEPES (pK_a = 7.5) for pH 7.0−8.5, HEPBS (pK_a = 8.3) for pH 8.5−9.0, and CHES (pK_a = 9.3) for pH 9.0−10.0. Buffer crossover experiments revealed no dependence on the buffer salt.

Choice of pH for Temperature Dependence Studies

Three factors were important in choosing the pH values for our studies of the temperature dependence of α-CT catalysis. The first was the hydrolytic reactivity of thiobenzyl esters. This was a concern because part of our analysis required measuring kinetic parameters for the α-CT-catalyzed hydrolysis of thiobenzyl esters which undergo significant nonenzymatic hydrolysis at pH >8. With this fact in mind, we chose an experimental pH of 7.0 or 7.5 for these studies. The second was the pH dependence of the kinetic parameters. This second factor was important because in the analysis of the data from our temperature dependence studies we needed to be able to calculate pH-independent kinetic parameters from experimental kinetic parameters that we intended to determine at a single pH value. This calculation of course requires knowledge of the pH dependence of the kinetic parameters. The third was the temperature dependence of pK_a values of active site residues and buffer salts. Protonation of α-CT's active site is exothermic, exhibiting a temperature-dependent pK_a of approximately −0.015 per degree Celsius (*3*, *4*). To compensate for this, we conducted our studies in HEPES buffer (pK_a = 7.55) for which $\Delta pK_a/\Delta°C = -0.014$, MES buffer ($pK_a$ = 6.15) for which $\Delta pK_a/\Delta°C = -0.011$, or PIPES buffer ($pK_a$ = 6.80) for which $\Delta pK_a/\Delta°C = -0.009$ (*5*). Thus, the pK_a of the buffer and α-CT change in concert with temperature variation, and thus, at any temperature, the α-CT reaction will be occurring at the same position on the pH−rate profile.

Kinetic Methods

p-Nitroanilide Hydrolysis. In a typical kinetic run, 80 μL of an appropriately diluted solution of stock peptide *p*-nitroanilide in DMSO was added to 2.00 mL of assay buffer in a 3 mL cuvette ($[DMSO]_o$ = 4%), and the cuvette was placed in the jacketed cell holder of a Perkin-Elmer Lambda 20 spectrophotometer. The desired reaction temperature was maintained to a tolerance of ±0.1 °C by a circulating water bath. After the reaction solution had reached thermal equilibrium (~5−10 min), an aliquot of stock α-CT was added to the cuvette to initiate the reaction. Reaction progress was monitored by the increase in absorbance at 410 nm (ϵ_{410} = 8800 M^{-1} cm^{-1}) that accompanies hydrolysis of the peptide *p*-nitroanilide substrate and release of *p*-nitroaniline. For each kinetic run, 100−3000 data points, corresponding to (time, absorbance) pairs, were collected by a personal computer interfaced with the spectrophotometer.

Thiobenzylester Hydrolysis. We used one of two methods to measure rates of thioester hydrolysis depending on the

[2] Abbreviations: Suc, *N*-succinyl; pNA, *p*-nitroanilide; Abu, α-aminobutyric acid; Nle, norleucine; α-CT, α-chymotrypsin; ONAA, *o*-nitroacetanilide; AChE, acetylcholinesterase; TST, transition-state theory; ZPE, zero-point energy; eu, entropy unit (calories per degree Celsius per mole).

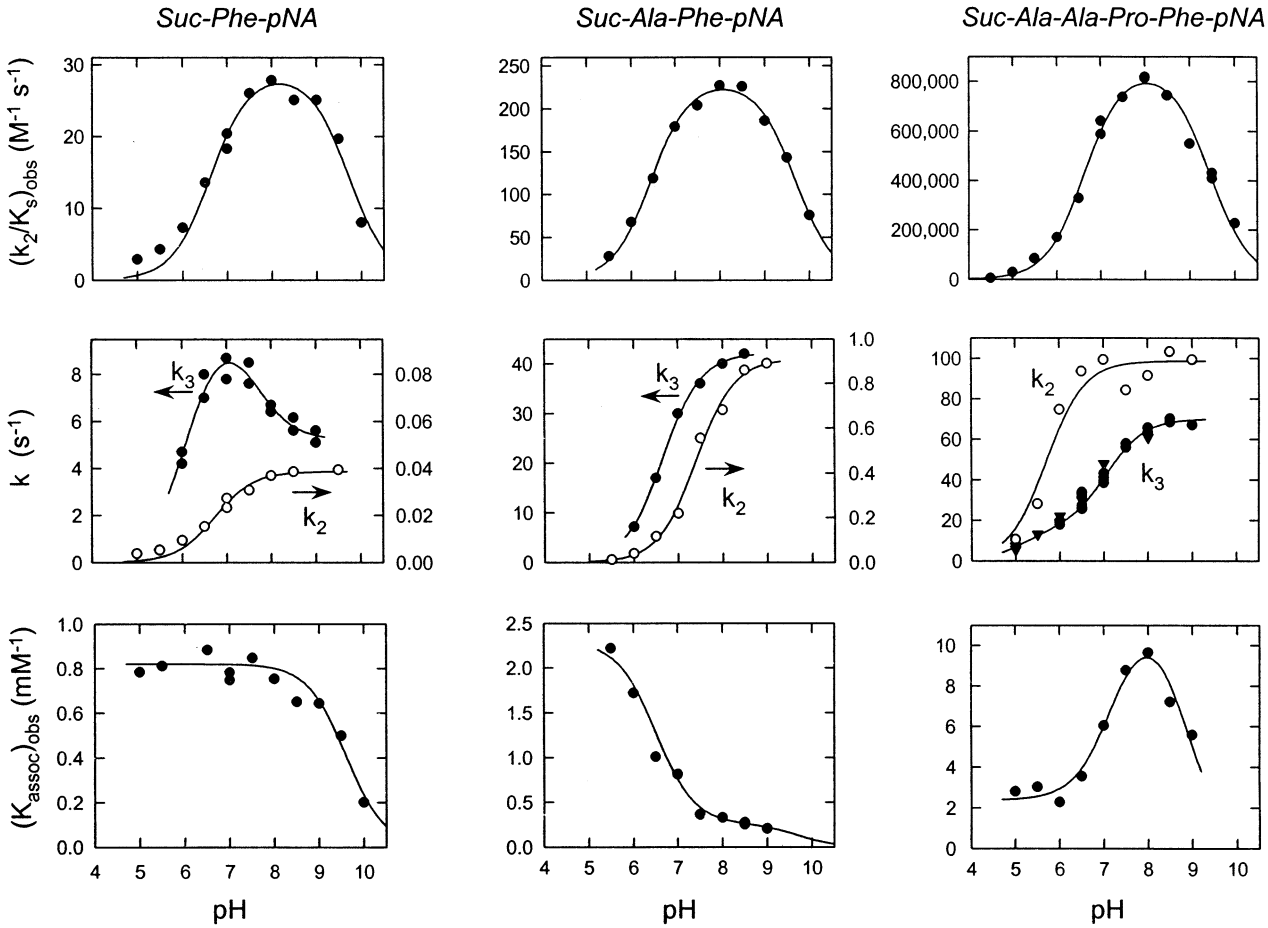

FIGURE 1: pH dependence of mechanistic rate constants for the α-CT-catalyzed hydrolyses of Suc-Phe-pNA, Suc-Ala-Phe-pNA, and Suc-Ala-Ala-Pro-Phe-pNA. Reactions were conducted in buffers containing 50 mM buffer salt, 500 mM NaCl, and 10 mM $CaCl_2$ at 30 °C.

reaction pH. At pH values of ≥6.0, we used a coupled assay in which the thiol product of thioester hydrolysis is allowed to react with DTNB that is added to the assay buffer. This coupling reaction produces a mixed disulfide and the chromophoric 2-nitro-4-carboxybenzoic acid ($\Delta\epsilon_{412} = 13\,000$ M^{-1} cm^{-1}). At pH <6.0, where reaction of thiol with DTNB is prohibitively slow, we monitored the decrease in absorbance at 250 nm that accompanies thiobenzylester hydrolysis ($\Delta\epsilon_{250} = -750$ M^{-1} cm^{-1}). In assays at pH >6, 40 μL each of an appropriately diluted solution of stock thiobenzylester and a 100 mM stock solution of DTNB in DMSO are added to 2.00 mL of assay buffer in a 3 mL cuvette ($[DTNB]_o$ = 1 mM, $[DMSO]_o$ = 4%). The rest of the kinetic method is essentially the same as that used for the nitroanilide substrates.

RESULTS

General Considerations for pH Dependence Studies. As briefly outlined in Materials and Methods, to accurately interpret the temperature dependencies of the mechanistic rate parameters K_s, k_2, and k_3 for α-CT-catalyzed hydrolysis of *p*-nitoranilides, we first needed to determine the pH dependencies of these parameters. This was done using a published method (*2*) that allows the calculation of mechanistic parameters from two pieces of information: (i) steady-state kinetic parameters k_c and K_m for nitroanilide hydrolysis and (ii) k_c values for hydrolysis of the corresponding thiobenzyl ester, for which acylation is rapid relative to deacylation and $k_c = k_3$ (see Scheme 1 and eq 2). This method is described below when we consider the hydrolysis of Suc-Ala-Ala-Pro-Phe-pNA.

At each pH, steady-state kinetic parameters, k_c/K_m, K_m, and k_c, were determined from the dependence of steady-state velocity on substrate concentration. Velocities were determined at no less than six substrate concentrations that varied from 50 to 5000 μM for Suc-Phe-pNA, from 10 to 2000 μM for Suc-Ala-Phe-pNA, and from 2 to 400 μM for Suc-Ala-Ala-Pro-Phe-pNA. For all three substrates at all pH values, the dependence of v_{ss} on $[S]_o$ could be fit to the Michaelis−Menten equation $v_{ss} = V_{max}[S]_o/(K_m + [S]_o)$, where $V_{max} = k_c[E]_o$. Specific details of analysis differ among the three systems and are presented individually below.

pH Dependence of the Kinetic Parameters for the α-CT-Catalyzed Hydrolysis of Suc-Phe-pNA. In preliminary experiments, we determined that the k_c values for the hydrolyses of Suc-Phe-pNA and Suc-Phe-SBzl are ∼0.03 and ∼8 s^{-1}, respectively (pH 7.5). Since the latter value of 8 s^{-1} is identical to k_3 for the hydrolysis of both substrates, we were able to equate K_m with K_s and k_c with k_2 for the hydrolysis of the anilide (see Scheme 1 and eqs 2 and 3). Thus, pH dependencies of steady-state parameters for the hydrolysis of Suc-Phe-pNA give direct access to pH dependencies of the mechanistic parameters K_s and k_2, while the pH dependence of k_c for hydrolysis of the thioester gives access to the pH dependence of k_3. These data, along with the data for the pH dependence of k_2/K_s, are plotted in Figure 1 and

Scheme 2: Minimal Kinetic Mechanism for the pH Dependence of the α-Chymotrypsin-Catalyzed Hydrolysis of Peptide *p*-Nitroanilide Substrates

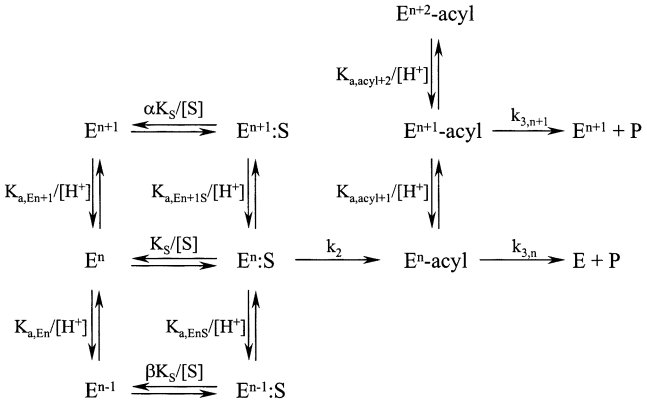

Table 1: Summary of pH Dependencies for α-Chymotrypsin Catalysis[a]

	Suc-Phe-pNA	Suc-Ala-Phe-pNA	Suc-Ala-Ala-Pro-Phe-pNA
k_2/K_s (M^{-1} s^{-1})	29 ± 1	233 ± 5	852000 ± 36000
$pK_{a,E^{n+1}}$	6.6 ± 0.1	6.45 ± 0.04	6.6 ± 0.1
pK_{a,E^n}	9.7 ± 0.1	9.69 ± 0.04	9.5 ± 0.1
k_2 (s^{-1})	0.039 ± 0.001	0.91 ± 0.03	98 ± 4
$pK_{a,E^{n+1}S}$	6.7 ± 0.1	7.4 ± 0.1	5.5 ± 0.2
pK_{a,E^nS}	>10	>10	>10
K_s (mM)	1.3 ± 0.1	3.8 ± 0.1	0.082 ± 0.003
α	1	0.11 ± 0.01	5 ± 1
β	>10	>10	>10
$pK_{a,acyl+2}$	6.1 ± 0.1	−	5.2 ± 0.2
$k_{3,n+1}$ (s^{-1})	11 ± 1	−	16 ± 2
$pK_{a,acyl+1}$	7.6 ± 0.2	6.66 ± 0.03	7.1 ± 0.1
$k_{3,n}$ (s^{-1})	5.2 ± 0.3	42 ± 1	71 ± 1

[a] pH dependencies were determined in buffers containing 50 mM buffer salt, 500 mM NaCl, and 10 mM $CaCl_2$ at 30 °C. Rate and equilibrium parameters correspond to those of the mechanism of Scheme 2. See the text for details of analysis.

were interpreted according to the mechanism of Scheme 2 as outlined below. This represents the minimal mechanism that can account for the pH dependencies of reaction of all three substrates and will be used as the interpretational framework for all of the pH dependencies of this study.

The pH dependence of k_2/K_s is bell-shaped and can be fit to the expression of eq 4

$$(k_2/K_s)_{obs} = \frac{k_2/K_2}{\frac{[H^+]}{K_{a,E^{n+1}}} + 1 + \frac{K_{a,E^n}}{[H^+]}} \quad (4)$$

which is derived from the kinetic mechanism of Scheme 2. The best-fit parameters from the nonlinear least-squares fit of the data for Suc-Phe-pNA to eq 4 are summarized in Table 1. Note in Figure 1 that at pH 5.0 and 5.5 the experimental values for $(k_2/K_s)_{obs}$ are greater than those predicted by eq 4 and the derived best-fit parameters. We believe that these deviations are not mechanistically significant but rather are due to the limited solubility of Suc-Phe-pNA at low pH. In general, acid dissociation constants that are derived from titration of k_2/K_s are due to catalytically essential ionizations of either substrate or enzyme. Since for Suc-Phe-pNA, and for all of the substrates of this study, the only ionizable group on the substrate has a pK_a of ∼4.5, the pH dependence of k_2/K_s must reflect ionizations of amino acid residues of the enzyme.

The pH dependence of k_2 is sigmoidal and was fit to the equation

$$(k_2)_{obs} = \frac{k_2}{\frac{[H^+]}{K_{a,E^{n+1}S}} + 1} \quad (5)$$

The best-fit parameters are summarized in Table 1. In this case, the acid dissociation constant, $K_{a,E^{n+1}S}$, reflects an ionization of the Michaelis complex that is critical for catalysis. We believe that the acidic ionization that is governed by K_{a,E^nS} was not observed in this experiment because it lies outside the pH range that was investigated here.

The rate expression for the dependence of K_{assoc} on pH is given in eq 6. Like k_2/K_s

$$(K_{assoc})_{obs} = \frac{(\alpha K_s)^{-1}}{1 + \frac{K_{a,E^{n+1}}}{[H^+]} + \frac{K_{a,E^{n+1}}K_{a,E^n}}{[H^+]^2}} + \frac{K_s^{-1}}{\frac{[H^+]}{K_{a,E^{n+1}}} + 1 + \frac{K_{a,E^n}}{[H^+]}} + \frac{(\beta K_s)^{-1}}{\frac{[H^+]^2}{K_{a,E^n}K_{a,E^{n+1}}} + \frac{[H^+]}{K_{a,E^n}} + 1} \quad (6)$$

the pH dependence of K_{assoc} (=$1/K_s$) reflects ionizations of the free enzyme, but unlike k_2/K_s, these ionizations will be observed only if they are important for substrate binding. We see that the shape of the dependence of $(K_{assoc})_{obs}$ on pH suggests that E^{n+1} and E^n bind Suc-Phe-pNA with essentially identical affinities so that α is near unity and the ionization that is governed by $K_{a,E^{n+1}}$ will be kinetically "invisible". Furthermore, β must be much greater than 10. These considerations allow us to set parameter constraints $\alpha = 1$, $\beta = 100$, and $pK_{aE^{n+1}} = 6.6$ and fit the data to eq 6 to arrive at best-fit values: $K_s = 1.3 \pm 0.1$ mM and $pK_{a,E^n} = 9.7 \pm 0.2$.

Finally, the pH dependence of k_3 is bell-shaped with a plateau on the alkaline side of the bell curve. The rate law that accounts for this behavior in the context of the mechanism of Scheme 2 is given in eq 7.

$$(k_3)_{obs} = \frac{k_{3,n+1}}{\frac{[H^+]}{K_{a,acyl+2}} + 1 + \frac{K_{a,acyl+1}}{[H^+]}} + \frac{k_{3,n}}{1 + \frac{[H^+]}{K_{a,acyl+1}} + \frac{[H^+]^2}{K_{a,acyl+1}K_{a,acyl+2}}} \quad (7)$$

When the data for Suc-Phe-pNA are fit to eq 7, the best-fit parameters summarized in Table 1 are obtained. The pH dependence of k_3 must reflect ionizations of the acyl−enzyme intermediate that are important for hydrolysis of this species.

pH Dependence of the Kinetic Parameters for the α-CT-Catalyzed Hydrolysis of Suc-Ala-Phe-pNA. For hydrolysis of Suc-Ala-Phe-pNA by α-CT, we found that k_3 is much larger than k_2 at all the pH values that were examined. This situation is identical to what we observed for Suc-Phe-pNA and thus allows us to again make the kinetic simplifications $K_m = K_s$ and $k_c = k_2$.

The pH dependencies of k_2/K_s and k_2 are shown in Figure 1. These data sets were analyzed using eqs 4 and 5, respectively, and the best-fit parameters are summarized in Table 1. The pH dependence of k_3 is also shown in Figure 1, but unlike the complex pH dependence of k_3 that we observed for hydrolysis of Suc-Phe-pNA, it has a simple sigmoidal shape and could therefore be analyzed using a rate expression of a form identical to eq 5. The best-fit values are as follows: $pK_{a,acyl+1} = 6.66 \pm 0.03$ and $k_{3,n} = 42 \pm 1$ s^{-1}. If we interpret these results in the context of the mechanism of Scheme 2, the simple shape of this dependence suggests that either $k_{3,n+1}$ is very small and less than ~ 1 s^{-1} or $pK_{a,acyl+2}$ is shifted to a value outside the range we used in this study; that is, $pK_{a,acyl+2}$ must be less than ~ 4.5. At this point, it is unclear which alternative obtains.

The dependence of K_{assoc} on pH (see Figure 1) suggests that the binding affinity between α-CT and Suc-Ala-Phe-pNA becomes weaker as the pH is increased; that is, according to Scheme 2, $\alpha \ll 1 \ll \beta$. And, as inspection of the data reveals, these changes in affinity are governed by pK_a values that are similar to those observed for the pH dependence of k_2/K_s, that is, 6.5 and 9.7. So, if pK_{a,E^n} and β are constrained to 9.7 and 100, respectively, the data can be fit to eq 6 with the following best-fit values: $K_s = 3.8 \pm 0.1$ mM, $\alpha K_s = 0.42 \pm 0.03$, and $pK_{a,E^{n+1}} = 6.5 \pm 0.1$. Note that the value of $pK_{a,E^{n+1}}$ determined here is identical to the value determined from the titration of k_2/K_s.

pH Dependence of the Kinetic Parameters for the α-CT-Catalyzed Hydrolysis of Suc-Ala-Ala-Pro-Phe-pNA. In contrast to those of Suc-Phe-pNA and Suc-Ala-Phe-pNA, the α-CT-catalyzed hydrolysis of Suc-Ala-Ala-Pro-Phe-pNA proceeds with values of k_2 and k_3 that are similar to one another and thus requires a more complex method for determining the pH dependence of its mechanistic rate constants. Our procedure here was to determine the pH dependencies of steady-state kinetic parameters for hydrolyses of both Suc-Ala-Ala-Pro-Phe-pNA and Suc-Ala-Ala-Pro-Phe-SBzl and then use these values together with eqs 8 and 9, which are rearranged forms of eq 2 and 3, respectively, to calculate values of k_2 and k_3 at the various pH values.

$$k_2 = \frac{k_3 k_c}{k_3 - k_c} \tag{8}$$

$$K_s = K_m \frac{k_2 + k_3}{k_3} \tag{9}$$

We start our analysis with k_2/K_s which can be accessed directly from observed values of k_c/K_m according to the equality expressed in eq 1. The pH dependence of k_2/K_s is bell-shaped (Figure 1) and could be fit to the expression of eq 4 (see Table 1 for best-fit parameters).

We also had direct access to k_3 values since these are equal to k_c values determined for the α-CT-catalyzed hydrolysis of Suc-Ala-Ala-Pro-Phe-SBzl. The dependence of k_3 on pH is shown in Figure 1 and was fit to eq 7 (see Table 1 for best-fit parameters).

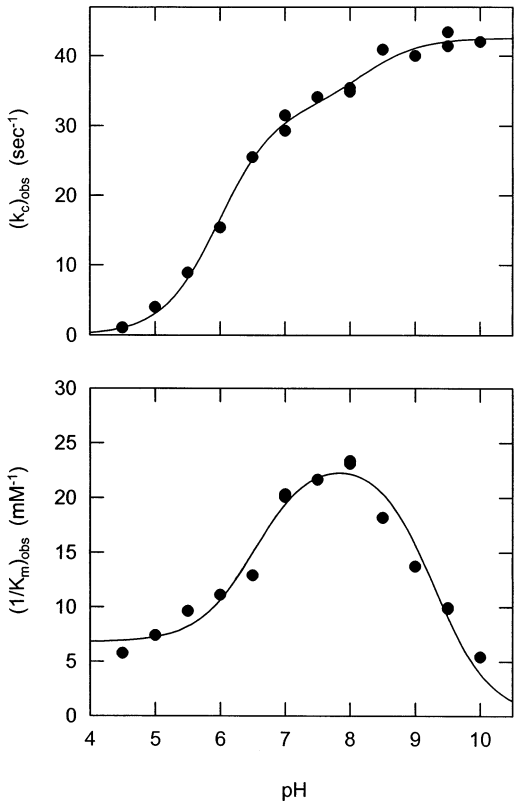

FIGURE 2: Dependence of $(k_c)_{obs}$ and $(1/K_m)_{obs}$ on pH for the α-CT-catalyzed hydrolysis of Suc-Ala-Ala-Pro-Phe-pNA. The solid lines through the data points were drawn using eqs 7 and 6, respectively, using the best-fit parameters summarized in the text. Reactions were conducted in buffers containing 50 mM buffer salt, 500 mM NaCl, and 10 mM $CaCl_2$ at 30 °C.

The final data sets that we require for calculation of the pH dependencies of k_2 and $1/K_s$ are the pH dependencies of k_c and $1/K_m$. These data are shown in Figure 2. We see from this figure that the shape of the dependence of k_c on pH is similar to the pH dependence of k_3 for the hydrolysis of Suc-Phe-pNA and depends on two pK_a values and a limiting, non-zero rate constant at alkaline pH. The line through the data was drawn using a rate expression similar in form to eq 7 and the best-fit parameters: $pK_{a,2} = 6.0 \pm 0.1$, $pK_{a,1} = 8.2 \pm 0.2$, $k_{c,n} = 33 \pm 1$ s^{-1}, and $k_{c,n+1} = 43 \pm 1$ s^{-1}. The pH dependence of $1/K_m$ was fit to a rate expression of a form identical to that of eq 6; the following best-fit parameters were found: $pK_{a,2} = 6.5 \pm 0.2$, $pK_{a,1} = 9.3 \pm 0.1$, $K_m = 42 \pm 2$ μM, $\alpha K_m = 148 \pm 22$ μM, and $\beta K_m > 1000$ μM. Note that the parameters that we calculated from the pH dependencies of k_c and $1/K_m$ are complex functions of K_s, k_2, k_3, and the acid dissociation constants.

Finally, then, with these pH dependencies for k_c, $1/K_m$, and k_3, we were able to calculate values of $(k_2)_{obs}$ and $(K_{assoc})_{obs}$ at the various experimental pH values using eqs 8 and 9. These data are summarized in Figure 1. The pH dependence of k_2 can be seen to be sigmoidal and can be fit to eq 5 (see Table 1 for fitting results). The pH dependence of $(K_{assoc})_{obs}$, like $(1/K_m)_{obs}$, was fit to eq 6: $pK_{a,E^{n+1}} = 7.2 \pm 0.2$, $pK_{a,E^n} = 8.9 \pm 0.2$, $K_s = 82 \pm 13$ μM, $\alpha K_s = 422 \pm 84$ μM, and $\beta K_s > 1000$ μM.

Table 2: Kinetic Parameters at pH 7.5 for the α-Chymotrypsin-Catalyzed Hydrolysis of Suc-Phe-pNA[a]

T (°C)	$k_c/K_m = k_2/K_s$ (M^{-1} s^{-1})	$K_m = K_s$ (μM)	$k_c = k_2$ (s^{-1})	k_3[b] (s^{-1})
10	6 ± 2	520 ± 31	0.0038 ± 0.0007	2.4 ± 0.1
20	19 ± 1	623 ± 12	0.0118 ± 0.0004	4.6 ± 0.1
30	37 ± 1	1080 ± 40	0.0398 ± 0.0022	8.7 ± 0.2
40	53 ± 3	1700 ± 250	0.0892 ± 0.0085	15.2 ± 0.7
50	65 ± 1	2680 ± 280	0.175 ± 0.016	26.5 ± 0.9

[a] Reactions were conducted at the indicated temperature in a pH 7.5 buffer containing 50 mM HEPES, 500 mM NaCl, and 10 mM $CaCl_2$. $[CT]_o = 1.0$ μM. Error limits are either standard errors of the mean ($n \geq 3$) or the deviation from the mean ($n = 2$), where n is the number of independent determinations of steady-state parameters. [b] k_3 is equal to k_c for the hydrolysis of the thiobenzyl ester, Suc-Phe-SBzl. Errors are from the cuve fitting of of the dependence of the initial velocity on $[S]_o$ to the Michaelis−Menten equation. In these experiments, $[CT]_o$ was lowered from 0.2 to 0.02 μM as the temperature and k_c increased.

Table 3: Kinetic Parameters at pH 6.0 for the α-Chymotrypsin-Catalyzed Hydrolysis of Suc-Ala-Phe-pNA[a]

T (°C)	k_c/K_m (M^{-1} s^{-1})	$K_m = K_s$ (μM)	$k_c = k_2$ (s^{-1})	k_3[b] (s^{-1})
10	5.4 ± 0.1	869 ± 10	0.0046 ± 0.0002	7.3 ± 0.2
20	21 ± 3	790 ± 10	0.0160 ± 0.0018	16.1 ± 0.6
30	46 ± 3	840 ± 10	0.0388 ± 0.0014	28.3 ± 0.9
40	74 ± 7	1170 ± 30	0.0863 ± 0.0089	53 ± 1
50	97 ± 4	1230 ± 40	0.133 ± 0.013	106 ± 2

[a] Reactions were conducted at the indicated temperature in a pH 6.0 buffer containing 50 mM MES, 500 mM NaCl, and 10 mM $CaCl_2$. $[CT]_o = 5.0$ μM. Error limits are either standard errors of the mean ($n \geq 3$) or the deviation from the mean ($n = 2$), where n is the number of independent determinations of steady-state parameters. [b] k_3 is equal to k_c for the hydrolysis of the thiobenzyl ester, Suc-Ala-Phe-SBzl. Errors are from the cuve fitting of the dependence of the initial velocity on $[S]_o$ to the Michaelis−Menten equation. In these experiments, $[CT]_o$ was lowered from 0.02 to 0.002 μM as the temperature and k_c increased. These data were collected at pH 7.5.

General Considerations for Temperature Dependence Studies. The principle experimental goal of this study was to determine mechanistic parameters K_s, k_2, and k_3 for the α-CT-catalyzed hydrolysis of Suc-Phe-pNA, Suc-Ala-Phe-pNA, and Suc-Ala-Ala-Pro-Phe-pNA as a function of temperature. Using methods that are similar to those outlined above, we were able to calculate these parameters from the measured steady-state parameters together with measured k_c values for the α-CT-catalyzed hydrolyses of the corresponding thiobenzyl esters.

Our studies of the pH dependence of the α-CT-catalyzed hydrolysis of Suc-Phe-pNA suggested that we should be able to conduct temperature dependence studies at pH 7.5. At this pH, Suc-Phe-SBzl is reasonably stable to spontaneous hydrolysis and the K_m is still manageably low (see Figure 1). Thus, we determined mechanistic rate constants at pH 7.5 which are summarized in Table 2. In contrast, for Suc-Ala-Phe-pNA, we needed to work at pH 6.0, which represented the best compromise of a low K_m value and a k_c that was sufficiently high to afford reasonable reactivity. Results of the temperature dependence for the α-CT-catalyzed hydrolysis of Suc-Ala-Phe-pNA at pH 6.0 are summarized in Table 3. Finally, we were able to conduct temperature dependence studies for the α-CT-catalyzed hydrolysis of Suc-Ala-Ala-Phe-Pro-Phe-pNA at pH 7.5. These data are summarized in Table 4.

Table 4: Kinetic Parameters at pH 7.5 for the α-Chymotrypsin-Catalyzed Hydrolysis of Suc-Ala-Ala-Pro-Phe-pNA[a]

T (°C)	k_c/K_m (mM^{-1} s^{-1})	K_m (μM)	k_c (s^{-1})	K_s[b] (μM)	k_2[c] (s^{-1})	k_3[d] (s^{-1})
10	251 ± 32	29 ± 3	7.3 ± 0.6	66 ± 12	16 ± 1	14 ± 2
20	767 ± 86	27 ± 1	28 ± 1	55 ± 10	41 ± 5	31 ± 1
30	1140 ± 150	35 ± 3	40 ± 2	96 ± 21	108 ± 8	64 ± 7
40	1530 ± 80	45 ± 5	72 ± 2	120 ± 3	171 ± 6	123 ± 12
50	1750 ± 170	73 ± 6	128 ± 16	172 ± 16	300 ± 46	224 ± 30

[a] Reactions were conducted at the indicated temperature in a pH 7.5 buffer containing 50 mM HEPES, 500 mM NaCl, and 10 mM $CaCl_2$. $[CT]_o$ ranged from 20 to 2 nM as the temperature was increased. [b] $K_s = K_m[(k_2 + k_3)/k_3]$. [c] $k_2 = k_3k_c/(k_3 - k_c)$. [d] k_3 is equal to k_c for the hydrolysis of the thiobenzyl ester, Suc-AAPF−SBzl. $[CT]_o$ ranged from 20 to 2 nM as the temperature was increased.

Temperature Dependencies of α*-Chymotrypsin Catalysis.* Tables 2−4 contain mechanistic kinetic parameters, K_s, k_2, and k_3, determined at five temperatures for the α-CT-catalyzed hydrolyses of Suc-Phe-pNA, Suc-Ala-Phe-pNA, and Suc-Ala-Ala-Pro-Phe-pNA. In this section, we analyze these data using a mechanism-independent approach; we postpone until the Discussion a more detailed and mechanism-driven analysis.

To analyze the temperature dependencies of $(K_s)_{obs}$ for interaction of the three substrates with α-CT, we first need to convert these observed values to pH-independent values, K_s (see Scheme 2). This was done using a rearranged form of eq 6 together with the experimental pH and the parameter estimates of Table 1. As it turns out, for reaction of Suc-Phe-pNA and Suc-Ala-Ala-Pro-Phe-pNA, this correction produces values that are essentially identical to those that were determined at pH 7.5. For Suc-Ala-Phe-pNA, the corrected and pH-independent values of K_s are ~5-fold larger than the values of $(K_s)_{obs}$ that were determined at the experimental pH of 6.0. Next, these values are inverted to transform them into association constants, K_{assoc}, and then multiplied by a standard-state concentration of 10^{-6} M. These unitless equilibrium constants, K_{assoc}', are then used to construct van't Hoff plots of $\ln(K_{assoc}')$ versus inverse temperature. For reaction of all three substrates, these plots are linear (Figure 3) and can be analyzed according to the simple thermodynamic expression of eq 10

$$\ln(K_{assoc}') = -\frac{\Delta H_{assoc}}{RT} + \frac{\Delta S_{assoc}}{R} \qquad (10)$$

where R is the universal gas constant and T is the temperature in kelvin. The following results are obtained: Suc-Phe-pNA, $\Delta H_{assoc} = -8.1 \pm 0.6$ kcal/mol and $\Delta S_{assoc} = -41 \pm 2$ eu; Suc-Ala-Phe-pNA, $\Delta H_{assoc} = -4.0 \pm 0.3$ kcal/mol and $\Delta S_{assoc} = -24 \pm 1$ eu; and Suc-Ala-Ala-Pro-Phe-pNA, $\Delta H_{assoc} = -4.4 \pm 0.6$ kcal/mol and $\Delta S_{assoc} = -24 \pm 2$ eu. For convenience of comparison, these values are also summarized in Table 5.

Transition-state theory provides the basis for our analysis of the temperature dependence of k_2 and k_3. According to TST, first-order rate constants for unimolecular processes

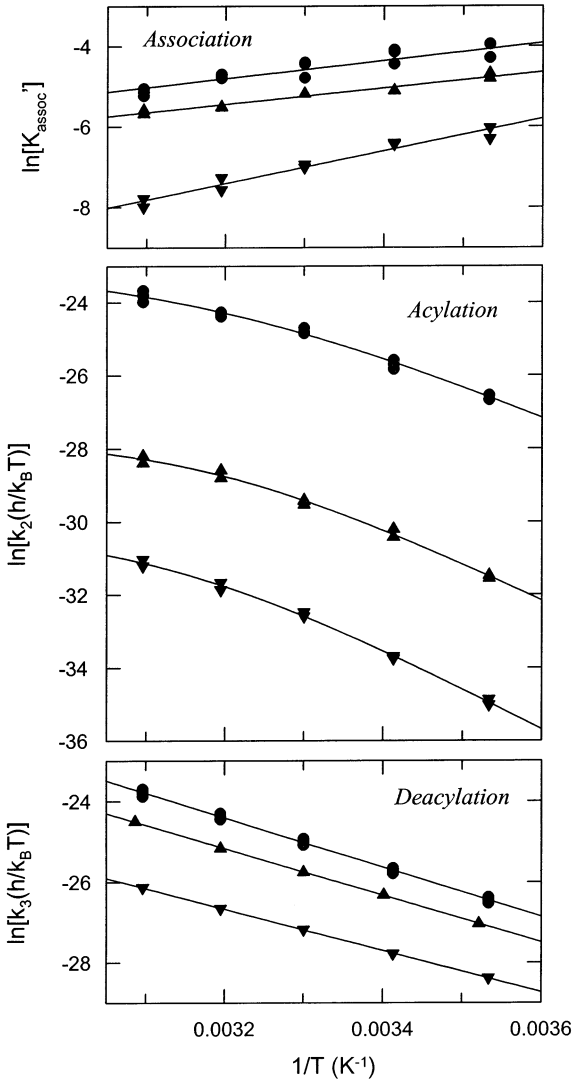

FIGURE 3: Temperature dependencies for α-CT catalysis. pH-independent mechanistic parameters, K_s, k_2, and k_3, for the α-CT-catalyzed hydrolysis of Suc-Phe-pNA (▼), Suc-Ala-Phe-pNA (▲), and Suc-Ala-Ala-Pro-Phe-pNA (●) were determined as outlined in the text and plotted here as dependencies on reciprocal temperature. In these plots, K_{assoc}' is the reciprocal of K_s multiplied by a standard-state substrate concentration of 10^{-6} M. The lines through the data sets for K_{assoc}' were drawn using eq 10 and the best-fit parameters summarized in the Results and Table 5. The lines through the data sets for k_3 were drawn using eq 13 and the best-fit parameters summarized in the Results and Table 5. And, finally, the lines through the data for k_2 were drawn using the thermodynamic expansion of eq 15 and the best-fit parameters of Table 9.

have the following dependence on temperature

$$k = \kappa \frac{k_B T}{h} \exp\left(-\frac{\Delta G^{\ddagger}}{RT}\right) \qquad (11)$$

where $\Delta G^{\ddagger}$, κ, k_B, h, and R are the Gibbs free energy of activation, the transmission coefficient (assumed here to be equal to 1), and the Boltzmann, Planck, and gas constants, respectively. The expression of eq 11 can be recast in quasi-thermodynamic form as eq 12

$$k = \frac{k_B T}{h} \exp\left[-\left(\frac{\Delta H^{\ddagger}}{RT} - \frac{\Delta S^{\ddagger}}{R}\right)\right] \qquad (12)$$

where $\Delta H^{\ddagger}$ and $\Delta S^{\ddagger}$ are the enthalpy and entropy of activation, respectively. Finally, eq 12 can be rearranged to eq 13:

$$\ln\left(k\frac{h}{k_B T}\right) = -\frac{\Delta H^{\ddagger}}{RT} + \frac{\Delta S^{\ddagger}}{R} \qquad (13)$$

Equation 13 predicts that a plot of $\ln[k(h/k_BT)]$ versus inverse temperature (i.e., an Eyring plot) will be linear with the slope and intercept proportional to $\Delta H^{\ddagger}$ and $\Delta S^{\ddagger}$, respectively.

Eyring plots of k_3 for the α-CT-catalyzed hydrolyses of Suc-Phe-pNA, Suc-Ala-Phe-pNA, and Suc-Ala-Ala-Pro-Phe-pNA were constructed using pH-independent values of k_3 that were calculated using a rearranged form of eq 7 together with the experimental pH and the parameter estimates of Table 1. These plots are linear (see Figure 3), and thus allow analysis using eq 13, yielding the following results: Suc-Phe-pNA, $\Delta H^{\ddagger} = 10.3 \pm 0.1$ kcal/mol and $\Delta S^{\ddagger} = -20.4 \pm 0.2$ eu; Suc-Ala-Phe-pNA, $\Delta H^{\ddagger} = 11.6 \pm 0.1$ kcal/mol and $\Delta S^{\ddagger} = -13.2 \pm 0.4$ eu; and Suc-Ala-Ala-Pro-Phe-pNA, $\Delta H^{\ddagger} = 12.2 \pm 0.2$ kcal/mol and $\Delta S^{\ddagger} = -9.7 \pm 0.7$ eu.

Eyring plots for k_2 were constructed using pH-independent k_2 values that were calculated using a rearranged form of eq 5 together with the parameter estimates of Table 1 and the experimental pH value. In contrast to the simple results we observed for k_3, these Eyring plots are all curved (see Figure 3) and require a more complex analysis. A purely phenomenological, mechanism-independent analysis is shown in Figure 4, where we plot $\Delta G^{\ddagger}$, $\Delta H^{\ddagger}$, and $-T\Delta S^{\ddagger}$ as a function of the temperature at which these parameters were calculated. Several points are noteworthy. (1) For any of the three substrates, $\Delta G^{\ddagger}$ does not vary with temperature and is equal to 19.8, 17.9, and 15.1 kcal/mol for acylation of α-CT by Suc-Phe-pNA, Suc-Ala-Phe-pNA, and Suc-Ala-Ala-Pro-Phe-pNA, respectively. (2) The dependencies of $\Delta H^{\ddagger}$ on temperature for reaction of Suc-Phe-pNA, Suc-Ala-Phe-pNA, and Suc-Ala-Ala-Pro-Phe-pNA have nearly identical slopes of −0.35, −0.31, and −0.30 kcal deg^{-1} mol^{-1}, respectively. (3) The dependencies of $-T\Delta S^{\ddagger}$ on temperature are also nearly identical for the two substrates with slopes of 0.35, 0.32, and 0.31 kcal deg^{-1} mol^{-1} for Suc-Phe-pNA, Suc-Ala-

Table 5: Thermodynamic Parameters for Reaction of Peptide *p*-Nitroanilides with α-Chymotrypsin

substrate	kinetic parameter	ΔG (kcal/mol)	ΔH (kcal/mol)	$-T\Delta S$ (kcal/mol)
binding[a]				
Suc-F-pNA	$K_{assoc} = 830$ M^{-1}	4.3	−8.0	12.4
Suc-AF-pNA	$K_{assoc} = 5300$ M^{-1}	3.2	−4.4	7.2
Suc-AAPF-pNA	$K_{assoc} = 8300$ M^{-1}	2.9	−4.4	7.3
acylation[b]				
Suc-F-pNA	$k_2 = 0.047$ s^{-1}	19.8	18.0	1.8
Suc-AF-pNA	$k_2 = 1.0$ s^{-1}	17.9	14.9	3.0
Suc-AAPF-pNA	$k_2 = 110$ s^{-1}	15.1	12.7	2.4
deacylation[c]				
Suc-F-pNA	$k_3 = 10$ s^{-1}	16.5	10.3	6.2
Suc-AF-pNA	$k_3 = 41$ s^{-1}	15.6	11.6	4.0
Suc-AAPF-pNA	$k_3 = 85$ s^{-1}	15.1	12.2	2.9

[a] Thermodynamic parameters for pH-independent values of K_a were calculated from linear van't Hoff plots with an $[S]_{standard-state}$ of 1×10^{-6} M and a T of 303 K (see Figure 3). [b] Activation parameters for pH-independent values of k_2 were taken from Figure 3 at a reference temperature of 303 K. [c] Activation parameters for pH-independent values of k_3 were calculated from the linear Eyring plot of Figure 3 using eq 13 ($T = 303$ K).

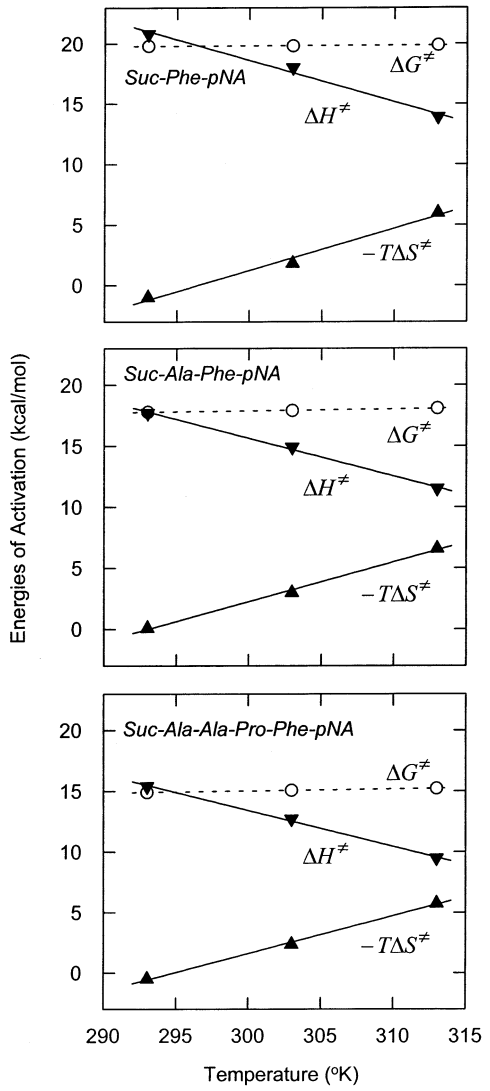

FIGURE 4: Temperature dependencies of the energies of activation, $\Delta G^{\ddagger}$, $\Delta H^{\ddagger}$, and $-T\Delta S^{\ddagger}$, for acylation of α-chymotrypsin (see the text for details).

Phe-pNA, and Suc-Ala-Ala-Pro-Phe-pNA, respectively. Finally, (4) the dependence of k_2 on peptide length is manifested entirely in the enthalpy of activation. That is, at any temperature, $\Delta\Delta G^{\ddagger}$ for any pair of substrates is approximately equal to $\Delta\Delta H^{\ddagger}$; $-T\Delta\Delta S^{\ddagger}$ is near zero. In the Discussion, we will provide a detailed analysis of these data and a mechanistic rationale that accounts for the temperature-dependent enthalpies and entropies of activation that we observe.

Temperature Dependence of Solvent Isotope Effects. Using the methods outlined above for calculating mechanistic kinetic parameters, we determined solvent isotope effects on k_2, k_3, and k_2/K_s for the α-CT-catalyzed hydrolysis of Suc-Ala-Ala-Pro-Phe-pNA at 20 and 50 °C. Relevant data are summarized in Table 6 and demonstrate that while the isotope effects for the three parameters do not differ statistically at the two temperatures, they do exhibit a trend that can be explained in the context of TST in which only the enthalpy of activation (∼ZPE) should vary with isotopic substitution; that is, $\Delta\Delta G^{\ddagger} = \Delta\Delta H^{\ddagger}$ and $\Delta\Delta S^{\ddagger} = 0$. For example, according to TST, the isotope effect on k_2 of 2.83 ± 0.45 at 50 °C would reflect a $\Delta\Delta H^{\ddagger}$ of 0.315 kcal/mol.

Table 6: Temperature Dependence of the Solvent Isotope Effect for the Chymotrypsin-Catalyzed Hydrolysis of Suc-Ala-Ala-Pro-Phe-pNA[a]

parameter	20 °C	50 °C
k_{2,H_2O} (s^{-1})	40.2 ± 4.7	269 ± 37
k_{2,D_2O} (s^{-1})	13.0 ± 1.1	95 ± 8
$^{D}k_2$	3.1 ± 0.4	2.8 ± 0.4
k_{3,H_2O} (s^{-1})	30.3 ± 1.8	234 ± 26
k_{3,D_2O} (s^{-1})	12.1 ± 0.2	101 ± 7
$^{D}k_3$	2.5 ± 0.2	2.3 ± 0.3
$(k_2/K_s)_{H_2O}$ (mM^{-1} s^{-1})	640 ± 45	1670 ± 133
$(k_2/K_s)_{D_2O}$ (mM^{-1} s^{-1})	357 ± 35	995 ± 65
$^{D}(k_2/K_s)$	1.8 ± 0.2	1.7 ± 0.2

[a] Reactions were conducted at the indicated temperature at pH and pD-equivalent 7.5. Buffer solutions contained 50 mM HEPES, 500 mM NaCl, and 10 mM $CaCl_2$. Each value represents the mean and standard deviation of three to six independent kinetic experiments, where a kinetic experiment comprises the determination and analysis of the dependence of steady-state velocity on no less than five substrate concentrations. Values for k_2, k_3, and k_2/K_s were calculated from the steady-state kinetic parameters as outlined in the text.

Table 7: Dependence of the Catalytic Efficiency on Substrate Chain Length for Serine Proteases

	k_2/K_s (M^{-1} s^{-1})	K_s (mM)	k_2 (s^{-1})	k_3 (s^{-1})
porcine pancreatic elastase[a]				
Ac-Ala-Pro-Ala-NH_2	21	4.2	0.09	–
Ac-Pro-Ala-Pro-Ala-NH_2	2100	3.9	8.5	–
human leukocyte elastase[b]				
Suc-Val-pNA	75	0.79	0.06	10
Suc-Pro-Val-pNA	580	0.72	0.42	11
Suc-Ala-Pro-Val-pNA	56000	0.81	43	13
Suc-Ala-Ala-Pro-Val-pNA	182000	0.24	43	13
bovine chymotrypsin				
Suc-Phe-pNA[c]	29	1.3	0.04	11
Suc-Ala-Phe-pNA[c]	233	3.8	0.91	42
Suc-Ala-Ala-Phe-pNA[d]	120000	–	–	–
Suc-Ala-Ala-Ala-Phe-pNA[d]	260000	–	–	–
Suc-Ala-Ala-Pro-Phe-pNA[c]	850000	0.1	98	71

[a] See ref *1*. [b] See ref *2*. [c] This work. [d] See ref *30*.

Given this value, we can calculate an isotope effect of 3.14 at 20 °C, which agrees with the experimental value of 3.09 ± 0.45.

DISCUSSION

The results of this study show that k_c/K_m for α-CT catalysis increases by more than 4 orders of magnitude as the substrate is lengthened from Suc-Phe-pNA to Suc-Ala-Ala-Pro-Phe-pNA. Similar dependencies of catalytic efficiency on peptide chain length have been observed for other serine proteases (see Table 7) and have been interpreted to suggest that these enzymes possess an extended active site with discrete subsites that can bind the amino acid residues of the peptide chain of the substrates. This interpretation is supported by X-ray crystallographic studies that document extensive interactions between bound peptides and extended substrate binding regions on these enzymes.

In a few cases, kinetic dissection of steady-state kinetic parameters has revealed that substrate chain length predominantly affects acylation and has little or no effect on binding or deacylation (Table 7). In the case presented here, increasing the length of the substrate from Suc-Phe-pNA to

Suc-Ala-Ala-Pro-Phe-pNA results in a 2300-fold increase in k_2 with only 10-fold increases in K_{assoc} and k_3. Results of this sort have been explained in terms of intrinsic binding energy and how it is utilized by proteases (*2*). Binding energy that is released from favorable interactions between peptide substrates and protease subsites is primarily utilized to stabilize catalytic transition states and not to stabilize reactant-state complexes, such as the Michaelis complex. It is these favorable transition-state interactions that are thought to pay the energetic price for catalysis (*6*, *7*).

If we apply these principles to the case presented here, we see that the dramatic dependence of k_2 on substrate chain length indicates that in proceeding from the Michaelis complex to the transition state for acylation, Suc-Ala-Ala-Pro-Phe-pNA establishes new contacts at remote subsites within the extended active site of α-CT. These new subsite interactions are, of course, not available to Suc-Phe-pNA and account for the observed $\Delta\Delta G^{\ddagger}$ of nearly 5 kcal/mol. Furthermore, these remote site interactions appear to be most important in the transition state for acylation and relatively unimportant in the Michaelis complex and the transition state for deacylation.

In an attempt to gain a greater understanding of this phenomenon, we determined the temperature dependencies of binding, acylation, and deacylation. As described in detail below, these studies not only allowed us to determine how the free energy changes for these three processes are distributed into their enthalpic and entropic components but also allowed mechanistic insights into acylation, due to the observation of unexpected kinetic complexity that occurs during acylation. As a prelude to the determination of the activation parameters for α-CT catalysis, we needed to determine pH dependencies for the various kinetic parameters.

pH Dependence of Catalysis by α-Chymotrypsin

Our understanding of the pH dependence of rate constants for reactions of serine proteases, in general, and α-CT, in particular, comes from studies of the hydrolysis of simple amides and esters of amino acids. For example, in a classic study by Bender (*8*), he observed the following pH dependencies for the α-CT-catalyzed hydrolysis of Ac-Phe-NH_2 (25 °C, ionic strength of 0.1 M): (i) bell shape for k_2/K_s with pK_a values of 6.5 and 8.5 for the acidic and basic limbs, respectively, (ii) bell shape for k_2 with pK_a values of 6.6 and 9.2, and (iii) sigmoid shape for k_3 with a pK_a of 6.8. Similar results have been found for other simple esters and amides (*3*, *4*, *9*). On the basis of a variety of biophysical studies, it has been possible to identify the imidazole moiety of the active site His-57 as the group with the pK_a of ~6.7. Given its assumed role as a general base catalyst, protonation of His-57 would be expected to generate an inactive form of the enzyme. Likewise, the pK_a of ~9 has been identified with disruption of an ion pair (*10*) between the amino group of Ile-16 and the carboxyl of Asp-194. This ion pair resides within the nonpolar interior of the protein upon activation of the zymogen and is critical for maintenance of the enzyme's catalytic activity.

With the exception of the pH dependence for deacylation, the pH dependencies that we observed for the three peptide *p*-nitroanilide substrates are in agreement with these previous results. pH dependencies of k_2/K_s are all bell-shaped and generate average pK_a values of 6.55 ± 0.09 and 9.63 ± 0.11 for the acidic and basic limb, respectively. The pH dependencies for k_2 exhibit acidic pK_a values that vary with substrate structure from 5.5 to 7.4 (see Table 1). Note that these studies could be conducted over a pH range that extended only to 9.0 or 9.5. Thus, for the three substrates of this study, we can conclude that the high-pH ionization (i.e., pK_{a,E^nS} of Scheme 2) must have a value greater than 10. In contrast to these simple pH dependencies for k_2, the pH dependencies for k_3 are complex and require at least two catalytically competent forms of the acyl−enzyme intermediate (see Scheme 2). At present, it is unclear how these acyl−enzyme forms differ and why such pH dependencies were not seen with simple esters and amides.

Thermodynamic Basis for α-Chymotrypsin's Subsite Specificity

Binding. The association constants for the binding of Suc-Ala-Phe-pNA and Suc-Ala-Ala-Pro-Phe-pNA to α-CT are similar and only 8-fold greater than K_{assoc} for Suc-Phe-pNA, corresponding to a $\Delta\Delta G_{assoc}$ of 1.2 kcal/mol (see Table 5). In the analysis of these ΔG_{assoc} values, the van't Hoff plots reveal that the very favorable enthalpy terms are more than offset by unfavorable entropy terms (Table 5). This implies that, within the active site, the hydrogen bonds and van der Waals interactions, which stabilize the Michaelis complex and contribute to a negative enthalpy of association, are energetically countered by restriction of the substrate's and enzyme's conformational mobility, which contribute to a negative entropy of association. Solvation effects must also play a role in this process. In solution, the hydrophobic groups of the substrates are surrounded by a shell of water molecules that is more ordered and has stronger hydrogen bonding than bulk water. This difference between shell and bulk water results in positive enthalpy and entropy contributions to the observed free energy of association for the transfer of all three substrates to the active site of α-CT.

One point of particular interest is that ΔH_{assoc} and $-T\Delta S_{assoc}$ are both much larger for Suc-Phe-pNA than they are for either Suc-Ala-Phe-pNA or Suc-Ala-Ala-Pro-Phe-pNA (Table 5). This observation suggests that in the Michaelis complexes of α-CT with the latter two substrates, the interactions between the enzyme and substrate are weaker and fewer in number than in the Michaelis complex formed from interaction of α-CT with Suc-Phe-pNA. Thus, the only reason that K_{assoc} is larger for Suc-Ala-Phe-pNA and Suc-Ala-Ala-Pro-Phe-pNA than it is for Suc-Phe-pNA is the more favorable entropy factor, which may reflect release of a greater number of "frozen" water molecules as the larger, more hydrophobic substrate binds to the active site. Another factor that must be at work here is the energetics of the release of the water molecules that line the extended active site, which will of course be different for the two substrates.

Acylation. For α-CT and other serine proteases, the rate of reaction within the Michaelis complex to form the acyl−enzyme intermediate shows a dramatic dependence on peptide substrate chain length. In this study, we demonstrate that extending the substrate from Suc-Phe-pNA to Suc-Ala-Ala-Pro-Phe-pNA is accompanied by a 2300-fold increase in k_2, reflecting a $\Delta\Delta G^{\ddagger}$ of nearly 5 kcal/mol (see Table 5). The temperature dependencies of k_2 for reaction of three

substrates reveal large values of $\Delta H^{\ddagger}$ that, overall, differ by ~5 kcal/mol, but small and nearly identical values of $\Delta S^{\ddagger}$. Thus, the observed increase in catalytic efficiency that is observed when Suc-Phe-pNA is extended to Suc-Ala-Ala-Pro-Phe-pNA is entirely enthalpic in origin. Since identical chemical transformations occur for these substrates, the large observed enthalpy difference must reflect enthalpy changes of the protein or protein−substrate complex that occur as the Michaelis complex is transformed into the activated complex for acylation.

One mechanism that can explain these results is catalysis by distortion. According to this mechanism, nucleophilic attack of the active site serine hydroxyl on the carbonyl carbon of the amide substrate can be facilitated if the scissile amide bond is twisted out of its stable, planar conformation. This distortion disrupts the resonance stabilization of the amide and renders the carbonyl moiety of the amide more ester-like and more reactive toward nucleophilic attack. A serine protease can effect catalysis by distortion if it can support a mechanism in which reaction progress from the Michaelis complex to the activated complex for acylation includes the conformational isomerization of the active site to a geometry that can only accommodate a twisted scissile amide bond. This enzyme conformation is presumably one of a large ensemble of energetically similar conformations that are sampled by the enzyme and are stabilized, and thus "selected", by substrates that can engage in extended subsite interactions. We see then that extended substrates which can engage in subsite interactions react faster than shorter substrates for which these interactions are not available and, therefore, cannot select the most reactive conformers of the protease.

Finally, this mechanistic proposal involving catalysis by distortion gains support from the three major findings of this study. (1) $\Delta G^{\ddagger}$ for acylation is dominated by the enthalpy term. This is expected for a mechanism involving catalysis by distortion where a large change in enthalpy is necessary to distort the amide linkage out planarity (*11*). Little or no change in entropy would need to occur if orientation of the substrate had occurred at the stage of the Michaelis complex. (2) Little change in K_s but a large increase in k_2 accompanies lengthening of the substrate. This is precisely what would be expected for a mechanism in which the role of subsite interactions is to select and stabilize enzyme conformations which promote distortion. Thus, subsite interactions are manifested in the transition state for acylation and not at the stage of the Michaelis complex. (3) The Eyring plots are convex. Of the four potential mechanisms that we will advance to explain this observation, at least three are consistent with a mechanism of catalysis by distortion (see below).

Deacylation. The data of Table 5 point to a small, positive dependence of k_3 on the peptide chain length of the substrate portion of the acyl−enzyme form. Curiously, as the chain length is extended from Suc-Phe-α-CT to Suc-Ala-Ala-Pro-Phe-α-CT and $\Delta G^{\ddagger}$ decreases from 16.5 to 15.1 kcal/mol, $\Delta H^{\ddagger}$ *increases* from 10.3 to 12.2 kcal/mol, indicating that if not for compensating entropy terms, k_3 would actually decrease with increasing peptide chain length.

One explanation for this behavior focuses on the relative stabilities of the three acyl−enzyme forms, Suc-Phe-α-CT, Suc-Ala-Phe-α-CT, and Suc-Ala-Ala-Pro-Phe-α-CT. One can imagine that increased chain length in this series might allow additional enthalpically favorable interactions to be established. If these interactions are manifested to a disproportionately greater degree in the acyl−enzyme intermediate than in the transition state for deacylation, we would see the observed dependence of $\Delta H^{\ddagger}$ on substrate chain length. In such a mechanism, values of $-T\Delta S^{\ddagger}$ would decrease as chain length increases if reaching the transition state from the acyl−enzyme forms of this series requires less organization. We see then that according to this mechanism, acyl−enzymes of specific substrates for α-CT are enthalpically stabilized and preorganized for deacylation.

Table 8: Summary of Kinetic Data for the Deacylation of Acyl Chymotrypsins[a]

acyl-α-CT	k_3 (s^{-1})	$\Delta G^{\ddagger}$	$\Delta H^{\ddagger}$	$-T\Delta S^{\ddagger}$
Suc-Ala-Ala-Pro-Phe-α-CT[b]	85	15.1	12.2	2.9
Suc-Phe-α-CT[b]	10	16.5	10.3	6.2
Ac-Phe-α-CT[c]	120	14.9	10.5	4.5
Ac-Nle-α-CT[d]	22	–	–	–
Ac-Leu-α-CT[d]	5	–	–	–
Ac-Abu-α-CT[c]	2	17.5	16.3	1.2
Ac-Gly-α-CT[d]	0.3	–	–	–

[a] Units of activation parameters are kilocalories per mole. $T = 303$ K. [b] This work. [c] See ref *3*. [d] See ref *12*.

We should note that the relative kinetic insensitivity to hydrolysis that we observe in proceeding from Suc-Phe-α-CT to Suc-Ala-Ala-Pro-Phe-α-CT is not a universal property of acyl-α-CTs. In fact, rate constants for hydrolytic deacylation of acyl-α-CTs derived from simple esters of amino acids (see Table 8) show a dramatic dependence on the identity of the amino acid side chain (*3*, *12*). For example, deacylation rate constants for Ac-Phe-α-CT and Ac-Abu-α-CT differ by a factor of 60. An analysis of the activation parameters for these two reactions reveals that the $\Delta\Delta G^{\ddagger}$ value of 2.6 kcal/mol results from a large $\Delta\Delta H^{\ddagger}$ value of 5.8 kcal/mol offset by a $-T\Delta\Delta S^{\ddagger}$ of −3.3 kcal/mol. These results suggest that in proceeding to their transition states for deacylation, Ac-Phe-α-CT undergoes a greater loss of conformational mobility than does Ac-Abu-α-CT.

We see then that kinetic discrimination among acyl-α-CTs does occur, but at the level of primary residue interactions and not at the level of peptide length. That is, during deacylation, the remote subsite interactions that were so crucial during acylation make relatively little kinetic or catalytic difference.

Origins of the Curved Eyring Plots for Chymotrypsin Acylation

In these studies, we observed convex Eyring plots for acylation of α-CT by all three substrates that we studied (Figure 1). Convex, or at least curved, Eyring plots are generally thought to have one of at least four causes. (1) For reactions proceeding through at least two sequential steps, convex plots will be observed if the rate-limiting step changes with temperature. (2) For one-step reactions, convex Eyring plots will occur if that step has a negative heat capacity of activation. (3) Mechanisms involving fluctuations among enzyme conformers can generate nonlinear Eyring plots. (4) Convex Eyring plots can be caused by a temperature-sensitive coupling of an enzyme conformational change to the chemical step of catalysis.

Scheme 3: Expanded Mechanism for Serine Protease Catalysis

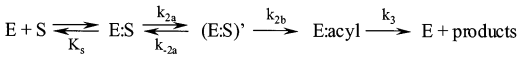

Table 9: Thermodynamic Parameters for the Acylation of α-Chymotrypsin by Substrates of the General Structure Suc-X-pNA (Model with Two Partially Rate-Limiting Steps[a])

X	k_2 (s^{-1})	$\Delta G_{2a}^{\ddagger}$	$\Delta H_{2a}^{\ddagger}$	$\Delta S_{2a}^{\ddagger}$	ΔG_{α}	ΔH_{α}	ΔS_{α}
F	0.04	19.9	2.4	8.35	0.7	17.8	56.4
AF	0.91	17.6	20.4	9.24	0.5	18.1	58.1
AAPF	98	14.8	19.9	10.2	0.4	14.6	47.2

[a] ΔG and ΔH values have units of kilocalories per mole, while ΔS values are in entropy units (i.e., calories per degree Celsius per mole). ΔG values were calculated at 303 K.

According to the first alternative, we would need to expand the general mechanism of serine protease catalysis (Scheme 1) to include a two-step process for acylation as shown in Scheme 3. The structural identity of the new intermediate (E:S)′ is discussed below.

According to the mechanism of Scheme 3, the experimentally observed acylation rate constant k_2 now reflects a more complex process involving partitioning of the intermediate species (E:S)′. Equation 14 is the rate expression for k_2:

$$k_2 = \frac{k_{2a}}{1+\alpha} \tag{14}$$

where

$$\alpha = \frac{k_{-2a}}{k_{2b}} \tag{15}$$

The expression of eq 14 can be recast in thermodynamic form and used to fit the data of Figure 3. The best-fit parameters are summarized in Table 9 and were used to draw the solid lines through the acylation data in Figure 3. The thermodynamic parameters of Table 9 indicate that, according to the model of Scheme 3, at low temperatures $\alpha < 1$ and $k_2 = k_{2a}$ while at high temperatures $\alpha > 1$ and $k_2 = (k_{2a}/k_{-2a})k_b$.

We believe it is unlikely that this mechanism accounts for the curved Eyring plots that we observe since we also observe nearly identical solvent isotope effects on k_2 at 20 and 50 °C (see Table 6). The small, statistically insignificant temperature dependence that we do observe is predicted by TST for a reaction with a single rate-limiting step (see the Results). If acylation proceeded through two or more partially rate-limiting steps, we would have likely observed isotope effects with a greater temperature dependence.

However, there is one explanation that could account for the observation of both a convex Eyring plot and a temperature-independent solvent isotope effect of 3.0, and involves a mechanism in which k_2 is partially rate-limited by the formation and subsequent decomposition of the tetrahedral intermediate (TI) through which acylation proceeds. As we described above, for this situation to arise, α must increase from 0.1 to 2 as the temperature is increased from 10 to 50 °C. We believe this is unlikely. Considerations of chemical reactivity for the tetrahedral intermediate of this reaction lead one to predict that α is likely to be much *larger* than 1, given the greater leaving group ability of an alcohol (i.e., Ser-195 hydroxyl) relative to an amine (i.e., nitrogen of the leaving group aniline). This expectation has experimental support in the alkaline hydrolysis of *p*-nitroacetanilide where the nonenzymatic equivalent of α is estimated to be between 200 and 800 (*13*).

Standing at odds with our best chemical expectations is a study of a mechanistically related system, the hydrolysis of *o*-nitroacetanilide by acetylcholinesterase, in which the investigators interpret their findings to support a mechanism in which acylation is, in fact, partially rate-limited by formation and decomposition of a tetrahedral intermediate (*14*). In this study, N^{15} isotope effects on k_c/K_m of 1.0119 ± 0.0005 and 1.0106 ± 0.0002 were observed in H_2O and D_2O, respectively. The solvent isotope effect on k_c/K_m was found to be 1.56 ± 0.3. The authors conclude from the small solvent isotope effect on the nitrogen isotope effect that acylation of AChE by ONAA is partially rate-limited by the three serial steps of the induced fit and the formation and decomposition of the tetrahedral intermediate.

So, while we are reluctant to strongly endorse a mechanism involving partially rate-limiting steps to account for the curvature of Eyring plots for acylation, neither can we exclude such a mechanism. Resolution of this issue awaits further experimentation.[3]

We turn now to the second mechanism, involving a single rate-limiting step with a negative heat capacity of activation, to account for our convex Eyring plots for acylation (*15*, *16*). Now, recall that in Results, we performed a mechanism-independent analysis of the curved Eyring plots and found that for the α-CT-catalyzed hydrolysis of all three substrates, $\Delta H^{\ddagger}$ and $\Delta S^{\ddagger}$ exhibit linear dependencies on temperature with slopes of approximately −320 cal deg^{-1} mol^{-1}. These slopes are, of course, equivalent to the heat capacity of activation. More accurate estimates for this parameter can be obtained by fitting the data sets to the expression of eq 16

$$\ln\left(k\frac{h}{k_B T}\right) = -\frac{\Delta H_o^{\ddagger}}{RT} + \frac{\Delta S_o^{\ddagger}}{R} + \frac{\Delta C_p^{\ddagger}}{R}\left[-1 + \frac{T_R}{T} + \ln\left(\frac{T}{T_R}\right)\right] \tag{16}$$

where $\Delta H_o^{\ddagger}$ and $\Delta S_o^{\ddagger}$ are the enthalpy and entropy of activation, respectively, at reference temperature T_R and $\Delta C_p^{\ddagger}$ is the heat capacity of activation. At a reference temperature of 30 °C, the best-fit values of Table 10 were determined. The lines drawn with the parameters and eq 10 can be superimposed on the lines of Figure 3.

Heat capacity changes of the magnitude calculated here are frequently found for protein folding reactions and have been interpreted to suggest large-scale conformational changes which bury hydrophobic surfaces with areas exceeding 500 $Å^2$ (*17*, *18*). This seems unlikely in the present case for which we anticipate relatively small changes in protein conformation. We should note that other explanations have been offered to account for non-zero heat capacity changes for

[3] The temperature dependence of the ^{15}N isotope effect for the α-CT-catalyzed hydrolysis of Suc-Phe-pNA is currently being studied by A. Hengge (Utah State University, Logan, UT) as part of a collaboration between our two laboratories.

Table 10: Thermodynamic Parameters for the Acylation of α-Chymotrypsin by Substrates of the General Structure Suc-X-pNA (Model with Single Rate-Limiting Step and Non-Zero Heat Capacity of Activation)[a]

X	k_2 (s^{-1})	$\Delta G^{\ddagger}$	$\Delta H^{\ddagger}$	$\Delta S^{\ddagger}$	$\Delta C_p^{\ddagger}$
F	0.04	19.9	17.4	−7.9	−292
AF	0.91	17.6	14.5	−12.1	−337
AAPF	98	14.8	12.5	−8.4	−236

[a] $\Delta G^{\ddagger}$ and $\Delta H^{\ddagger}$ values have units of kilocalories per mole, while $\Delta S^{\ddagger}$ and $\Delta C_p^{\ddagger}$ values are in entropy units (i.e., calories per degree Celsius per mole). $\Delta G^{\ddagger}$ values were calculated at 303 K.

Table 11: Thermodynamic Parameters for the Acylation of α-Chymotrypsin by Substrates of the General Structure Suc-X-pNA (Model with Parallel Paths to Product and Conformational Isomerization of the Michaelis Complex)[a]

X	k_2	$\Delta G_c^{\ddagger}$	$\Delta H_c^{\ddagger}$	ΔS_c*	ΔG_2*	ΔH_2*	ΔS_2*	$\Delta G_{12}^{\ddagger}$	$\Delta H_{12}^{\ddagger}$	$\Delta S_{12}^{\ddagger}$
F	0.04	18.4	16.9	−4.8	0.4	18.6	60.0	−1.4	21.4	75.1
AF	0.91	17.2	15.3	−6.4	0.0	18.2	59.9	−1.3	22.9	79.8
AAPF	98	14.1	12.9	−4.0	−0.3	18.9	63.3	−1.6	21.9	77.4

[a] k_2 has units of inverse seconds; ΔG and ΔH values have units of kilocalories per mole, while ΔS values are in entropy units (i.e., calories per degree Celsius per mole). ΔG values were calculated at 303 K.

reactions of proteins (*19*, *20*). It has been argued that the cooperative and multiple weak interactions that characterize hydrogen bonding networks within protein matrices as well as the quantum confinement that may occur at active sites may both cause large, negative heat capacity changes. However, these effects have been discussed in the context of protein folding and ligand binding reactions, respectively, and it is unclear at present if such effects can cause a $\Delta C_p^{\ddagger}$ of the magnitude observed here for catalytic turnover.

The third explanation for nonlinear Eyring plots involves catalytically important enzyme conformational fluctuations. To account for convex Eyring plots, these conformational isomers must exist as unstable intermediates on multiple, parallel reaction paths from the Michaelis complex to product, and these conformers must be in equilibrium with one another. If an equilibrium does not exist among the conformers, this mechanism reduces to one involving several independent paths to product and would generate concave Eyring plots. In essence, this third explanation represents a "preorganization" mechanism in which the conformational change of the Michaelis complex might be viewed as adjusting the active site residues for optimal reaction with bound substrate. While this is an interesting mechanism, it cannot account for the results in this paper. Recall that curved Eyring plots are observed only for acylation; the van't Hoff plots for K_{assoc} are linear. Analysis of this mechanism shows that it predicts nonlinear temperature dependencies for both acylation and substrate binding.

The fourth and final mechanism that we will consider involves the coupling of protein conformational isomerization to the reaction coordinate during the transformation of the Michaelis complex to product. While this is not a new idea (*21*−*25*), interest in it has recently been renewed with the observation of the apparent coupling of protein motions to active site hydrogen tunneling in a number of hydrogen transfer reactions (*26*, *27*).

The specific model we shall explore is shown in the MARS diagram of Scheme 4. According to this model, the

Scheme 4: Map of Alternate Routes (MARS) Diagram for the Coupling of Protein Conformational Isomerization to Active Site Chemistry[a]

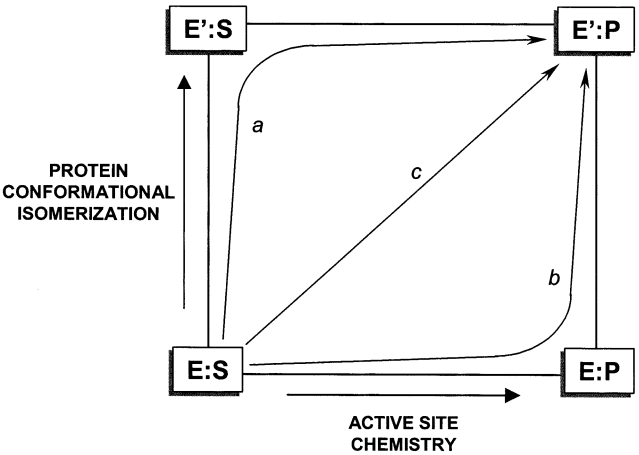

[a] Path a represents a mechanism in which conformational isomerization of the enzyme precedes chemistry and represents the preorganization mechanism described in the text. Path b is a mechanism in which isomerization of the enzyme follows chemistry. Path c is a concerted mechanism in which conformational isomerization of the protein is coupled to active site chemistry.

Michaelis complex E:S has the potential for three reactions: chemical conversion to E:P, protein isomerization to E′:S, or transformation to E′:P in which chemistry is coupled to protein isomerization. When we say that chemistry is coupled to isomerization, we mean not only that these two processes occur in a concerted fashion but also that chemistry occurs at an accelerated rate at the expense of protein isomerization. This is expressed in the free energy relationship of eq 17

$$\Delta G_c^{\ddagger} = \Delta G_{chem}^{\ddagger} - \gamma(\Delta G_{chem}^{\ddagger} - \Delta G_{isom}^{\ddagger}) \quad (17)$$

where $\Delta G_c^{\ddagger}$ is the free energy of activation for the observed, coupled reaction governed by k_c, $\Delta G_{chem}^{\ddagger}$ is the free energy of activation for chemical conversion of E:S to E:P governed by k_{chem}, $\Delta G_{isom}^{\ddagger}$ is the free energy of activation for protein isomerization of E:S to E′:S governed by k_{isom}, and γ is a coupling constant that can range from 0 to 1.

We see from the expression of eq 17 that coupling of chemistry to a conformational fluctuation of the protein allows the rate of the chemical process to increase by a factor that is related to the free energy difference between uncoupled active site chemistry and conformational isomerization. If coupling is inefficient and little of this energy difference can be used to accelerate chemistry, γ approaches 0. However, if the coupling process is efficient, much of the energy difference can be productively utilized and γ approaches 1. A convex Eyring plot will result only if γ is temperature-dependent and decreases with increasing temperatures; a temperature-independent coupling constant will only result in a linear Eyring plot. A similar model has been presented by Demchemko (*28*), who posits the expression of eq 18 to explain convex Arrhenius plots for enzymatic reactions.

$$k_{cat} = Ae^{-E_a \pm E_a^{dyn}(T)/RT} \quad (18)$$

In this equation, $E_a^{dyn}(T)$ is a temperature-dependent activa-

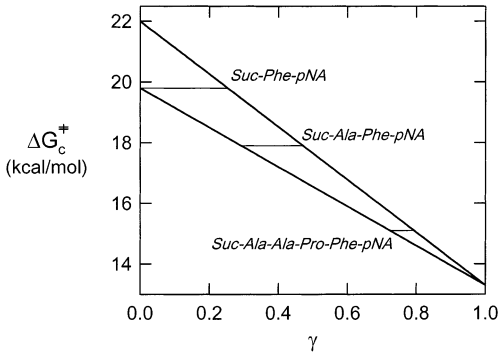

FIGURE 5: Dependence of the free energy of activation for acylation of α-CT on the coupling of protein conformational isomerization to active site chemistry according to eq 18. Free energies of activation were calculated with a T of 30 °C.

tion energy for protein dynamical processes that are coupled to active site chemistry.

Apart from the insight this model might give us concerning the origins of our curved Eyring plots, this model also addresses underlying mechanisms that give rise to α-CT's substrate selectivity. In general, for enzymatic reaction of a series of substrates at a single temperature, eq 17 predicts a linear dependence of $\Delta G_c^{\ddagger}$ on γ if the substrates of this series share similar values of $\Delta G_{chem}^{\ddagger}$ and $\Delta G_{isom}^{\ddagger}$. The plot of $\Delta G_c^{\ddagger}$ versus γ would have a slope equal to $-(\Delta G_{chem}^{\ddagger} - \Delta G_{isom}^{\ddagger})$ and limiting values of $\Delta G_{chem}^{\ddagger}$ and $\Delta G_{isom}^{\ddagger}$ when γ equals 0 and 1, respectively.

To construct such a plot for the three reactions of this study, we first need to assign reasonable estimates to $\Delta G_{chem}^{\ddagger}$ and $\Delta G_{isom}^{\ddagger}$. For $\Delta G_{isom}^{\ddagger}$, we assume a value of 13.3 kcal/mol which corresponds to a first-order rate constant of 1800 s^{-1}. This value is equal to k_2 for reaction of α-CT with the ester substrate Ac-Phe-OEt and is thought to be the upper limit for α-CT acylation, possibly corresponding to rate limitation by an enzyme conformational change (*29*). Thus, it is not unreasonable to assign this value to k_{isom}. A single value could not be reasonably assigned to $\Delta G_{chem}^{\ddagger}$; therefore, we allowed values to range from 19.8 to 22.0 kcal/mol. The former corresponds to the rate constant for acylation by Suc-Phe-pNA ($k_2 = 0.047$ s^{-1}), while that latter is the upper limit for the acylation of α-CT by *p*-nitroacetanilide[4] ($k_2 \leq 0.001$ s^{-1}). Taken together, these limits for $\Delta G_{chem}^{\ddagger}$ and $\Delta G_{isom}^{\ddagger}$ allow us to define the following ranges of γ values for the three substrates of this study (see Figure 5): $0 < \gamma < 0.25$ for Suc-Phe-pNA, $0.3 < \gamma < 0.5$ for Suc-Ala-Phe-pNA, and $0.7 < \gamma < 0.8$ for Suc-Ala-Ala-Pro-Phe-pNA. Thus, there appears to be a direct correlation between peptide chain length and the efficiency of coupling. To explain this, we propose that as peptide length increases, additional subsites of α-CT's extended active site are occupied and more efficiently engage the coupling mechanism between chemistry and conformational isomerization. This increased level of coupling lowers the overall free energy barrier for acylation.

Summary

In this study, we examined α-CT's selectivity toward peptide substrates of increasing chain length and found that while α-CT does express some discrimination among these substrates during binding and deacylation, the most dramatic effect is seen during acylation where k_2 increases by a factor of 2500 as the substrate is extended from Suc-Phe-pNA to Suc-Ala-Ala-Pro-Phe-pNA. The temperature dependence of k_2 reveals that this rate enhancement is entirely enthalpic in origin and led us to suggest a mechanism for acylation involving catalysis by distortion in which nucleophilic attack of the active site serine is facilitated by an enzyme conformation-induced twisting of the scissile amide bond out of its stable, planar geometry. A critical feature of this mechanism is the conformational isomerization that must occur as Michaelis complex progresses to the activated complex for acylation. Furthermore, this conformational isomerization must be sensitive to the length of peptide substrates. The temperature dependence of k_2 also reveals that the process governed by this rate constant is complex, possibly involving a coupling between active site chemistry and protein conformational isomerization. Taken together, this analysis of acylation suggests that extended substrates which can engage in subsite interactions are able to efficiently trigger the coupling mechanism between chemistry and a conformational isomerization that distorts the substrate and thereby promotes nucleophilic attack.

[4] Unpublished data of R.L.S.

NOTE ADDED AFTER ASAP POSTING

In the version of this article published on the Web 02/28/03, Scheme 1 was incorrect. Two R′−NH groups in the acylation and deacylation steps have been changed to R groups. The corrected version was published 03/18/03.

REFERENCES

1. Thompson, R. C., and Blout, E. R. (1973) *Biochemistry 12*, 51.
2. Stein, R. L., Strimpler, A. M., Hori, H., and Powers, J. C. (1987) *Biochemistry 26*, 1301−1305.
3. Dorovska-Taran, V., Montcheva, R., Gulubova, N., and Martinek, K. (1982) *Biochim. Biophys. Acta 702*, 37−53.
4. Kunugi, S., Hirohara, H., and Ise, N. (1979) *J. Am. Chem. Soc. 101*, 3640−3646.
5. Copeland, R. A. (2000) in *Enzymes: A Practival Introduction to Structure, Mechanism, and Data Analysis*, pp 242, Wiley-VCH, New York.
6. Fersht, A. R. (1974) *Proc. R. Soc. London, Ser. B 187*, 397−407.
7. Jenks, W. P. (1975) *Adv. Enzymol. Relat. Areas Mol. Biol. 43*, 219−410.
8. Bender, M. L., Clement, G. E., Kezdy, F. J., and Hck, H. A. (1964) *J. Am. Chem. Soc. 86*, 3680−3689.
9. Hammond, B. P., and Gutfreund, H. (1955) *Biochem. J. 62*, 187−194.
10. Bender, M. L., and Killgeffer, J. V. (1973) *CRC Crit. Rev. Biochem.*, 149−199.
11. Harrison, R. K., and Stein, R. L. (1992) *J. Am. Chem. Soc. 114*, 3464−3471.
12. Ingles, D. W., and Knowles, J. R. (1967) *Biochem. J. 104*, 369−377.
13. Stein, R. L., Fujihara, H., Quinn, D. M., Fischer, G., Kuellertz, G., Barth, A., and Schowen, R. L. (1984) *J. Am. Chem. Soc. 106*, 1457−1461.
14. Rao, M., Barlow, P. N., Pryor, A. N., Paneth, P., O'Leary, M. H., Quinn, D. M., and Huskey, P. (1993) *J. Am. Chem. Soc. 115*, 11676−11681.
15. Colen, A. H., Medary, R. T., and Fisher, H. F. (1981) *Biopolymers 20*, 879−889.
16. Rubach, J. K., Ramaswamy, S., and Plapp, B. V. (2001) *Biochemistry 40*, 12686−12694.
17. Goldberg, J. M., and Baldwin, R. L. (1998) *Biochemistry 37*, 2556−2463.

18. Fersht, A. R. (1999) in *Structure and Mechanims in Protein Science: A Guide to Enzyme Catalysis and Protein Folding*, Chapter 18, W. H. Freeman and Co., New York.
19. Cooper, A. (2000) *Biophys. Chem. 85*, 25−39.
20. Cooper, A., Johnson, C. M., Lakey, J. H., and Nollman, M. (2001) *Biophys. Chem. 93*, 215−230.
21. Lumry, R., and Biltonen, R. (1969) in *Structure and Stability of Biological Macromolecules* (Fasman, G., Ed.) Chapter 2, Dekker, New York.
22. Careri, G., Fasella, P., and Gratton, E. (1979) *Annu. Rev. Biophys. Bioeng. 8*, 69−97.
23. Welch, G. R., Somogyi, B., and Damjanovic, S. (1982) *Prog. Biophys. Mol. Biol. 39*, 109−146.
24. Somogyi, B., Welch, G. R., and Damjanovic, S. (1984) *Biochim. Biophys. Acta 768*, 81−112.
25. Welch, G. R. (1986) *The Fluctuating Enzyme*, John Wiley & Sons, New York.
26. Antoniou, D., Caratzoulas, S., Kalyanaraman, C., Mincer, J. S., and Schwartz, S. D. (2002) *Eur. J. Biochem. 269*, 3102−3112.
27. Knapp, M. J., and Klinman, J. P. (2002) *Eur. J. Biochem. 269*, 3113−3121.
28. Demchenko, A. P. (1997) *Comments Mol. Cell. Biophys. 9*, 87−112.
29. Brandt, K. G., Himoe, A., and Hess, G. P. (1967) *J. Biol. Chem. 242*, 3973−3982.
30. Boudier, C., Jung, M. L., Stambolieva, N., and Bieth, J. G. (1981) *Arch. Biochem. Biophys. 210*, 790−793.

BI020668L